



Roll-to-roll treatment of silk thread by a compact, single-step cold atmospheric plasma: hydrophobicity and mechanical properties

F. Sohbatzadeh^{1,2} · F. Shafei¹ · E. Shakerinasab¹ · M. Khajvand Salehan¹ · M. Ghasemi^{1,2}

Received: 7 April 2020 / Accepted: 12 June 2020 / Published online: 26 June 2020
© Springer-Verlag GmbH Germany, part of Springer Nature 2020

Abstract

In this study, the hydrophilic silk thread was changed to a hydrophobic surface by a compact cold atmospheric plasma (CAP) using Ar/C₆H₁₄ mixture as the working precursor. To test the hydrophobicity of the treated samples, water repellent examinations were performed and the static water contact angle of 139.62° was obtained. The durability of hydrophobicity was investigated using washing cycles and the aging effect. The color test of the samples was performed in CIELAB color space showing good stability in the silk color. To characterize the morphology of the processed samples, the changes in chemical bonds on the surface, deposited thin layer and redistribution of the atomic content on the surface were performed by atomic force microscopy, X-ray photoelectron spectroscopy, field emission scanning electron microscopy, energy-dispersive spectroscopy and X-map analyses, respectively. The CAP key parameters were investigated by the voltage–current profiles and optical emission spectroscopy. Moreover, the mechanical properties of the processed silk threads such as breaking strength, elongation, and extension were found to be improved. The results of this work could be used in the textile factory to modify the silk threads before or after dyeing, as well as for other fibers like wool and polyesters.

Keywords Cold atmospheric plasma · Ar/C₆H₁₄ atmospheric plasma · Hydrophobic silk thread · Plasma-based textile processing

1 Introduction

Silk is one of the popular fabrics for apparel because of its unique properties such as elegant appearance, softness, superior wear comfort, warmth, and biodegradability properties [1]. Although silk is valued for its unique properties, there are some disadvantage such as low printability and hydrophilicity that can be modified. Plasmas are acknowledged to be uniquely effective surface engineering tools to improve the surface properties of silk fabrics. An important advantage of plasma processing compared to the other apparatus is that it avoids liquid effluents and save large quantities of chemical composition and energy [2–4]. Also,

plasma processing does not change the bulk properties of the textiles and only modifies the material surface [5, 6]. Zhang et al. used the dielectric barrier discharge with ambient gas plasma to investigate the physical–morphological and chemical properties of the silk fabric for inkjet printing. The results proved that the modified silk has a deeper color, darker shade, and larger saturation compared to that of the pristine one [7].

Among different properties of silk fabrics, hydrophobicity is one of the issues of great interest in the textile industry. The hydrophobic silk fabrics are a class of textiles with the ability to remove any debris or bacteria from their surfaces as well as water-repellent property. There are two types of plasma systems for the hydrophobic treatment of the silk surface: low-pressure and atmospheric pressure plasma systems. The hydrophobicity properties of silk at low pressure have been studied by many research groups [8–11]. Rani et al. used a low-pressure plasma-enhanced chemical vapor deposition with the use of plasma-polymerized hexamethyl-disiloxane (HMDSO) to deposit a hydrophobic coating on the silk fabric. The results showed that the water contact angle of the silk increases from 0° to 140° [8]. Hodak et al.

✉ F. Sohbatzadeh
f.sohbat@umz.ac.ir

¹ Department of Atomic and Molecular Physics, Faculty of Basic Sciences, University of Mazandaran, Babolsar, Islamic Republic of Iran

² Plasma Technology Research Center, Faculty of Basic Sciences, University of Mazandaran, Babolsar, Islamic Republic of Iran

used a low-pressure inductively coupled SF_6 plasma with a frequency of 13.56 MHz to increase the hydrophobicity properties of the silk fabric. The results proved that water contact angles of the surface increase from 0 to 145 [4]. Furthermore, there have been a number of studies for the deposition of hydrophobic coatings on silk at atmospheric pressure [2, 12, 13]. Teli et al. used atmospheric pressure plasma system in the presence of helium–fluorocarbon (He–FC) gases to improve the hydrophobicity of the silk fabric. According to the results, after the plasma deposition, the fabric turned into a hydrophobic surface [2].

In previous works, we used cold atmospheric pressure dielectric barrier discharge plasma to hydrophobic deposition on cotton fabric [14]. In that work, we produced water repellent cotton fabric after 20 min of plasma treatments by $\text{Ar}/\text{C}_6\text{H}_{14}$ gas mixture (as low-cost and environmentally friendly precursor materials). The device operates at atmospheric pressure and does not require vacuum instrumentation. Using this DBD configuration, we surprisingly achieved a super-hydrophobic cotton fabric that can be used as oil/water filters [14]. The improvements in such devices are important issues in the textile industry.

In this work, to develop previous works, we changed the geometry of electrodes to produce a cold atmospheric pressure plasma with a different configuration with $\text{Ar}/\text{C}_6\text{H}_{14}$ gas

mixture to deposit a hydrophobic coating on silk thread. The new apparatus is more efficient and has many advantages compared to the other atmospheric pressure plasmas that are used for thread processing. The process is fast, single step, and roll to roll, which could be used in the textile industry to produce functional silk thread. The device is compact and could be installed before or after dyeing the fibers in the factory. The method could be used for the treatment of any type of thread. An important advantage of using this method is that the breaking strength, elongation, and extension of the samples were enhanced after the treatments. Another important advantage of this method is that the color of the samples did not change after the plasma processing.

2 Material and method

2.1 Experimental setup

A schematic diagram of the atmospheric pressure plasma with *n*-hexane precursor is shown in Fig. 1. As can be seen, the plasma device consisted of a copper tube and ring and a quartz housing. The copper tube served as the power electrode having an inner and outer diameter of 1.4 and 2.6 mm, respectively. This electrode was inserted into the quartz

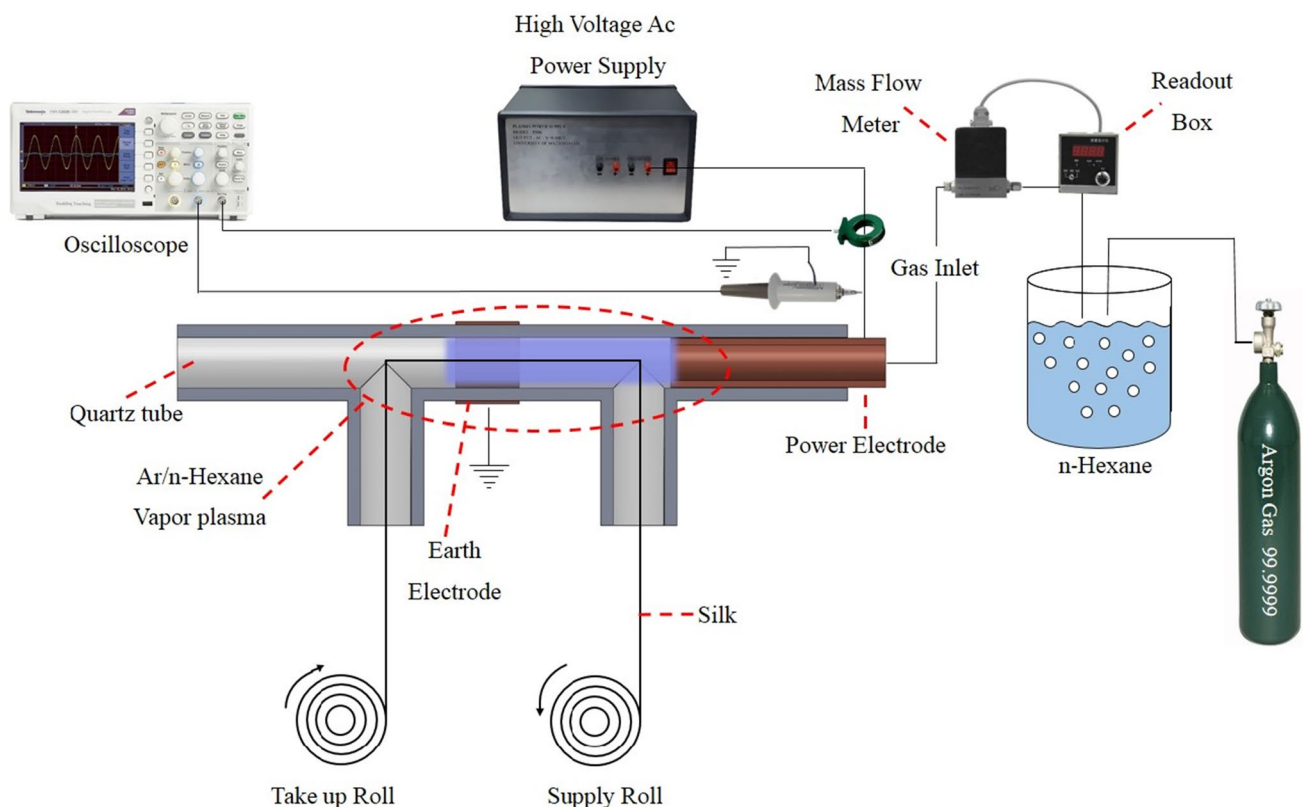


Fig. 1 Schematic diagram of the experimental setup

housing to direct the working gas mixture toward the plasma gap. A 6 mm copper foil wrapped around the quartz tube served as the ground electrode. The distance between the power and ground electrodes was fixed at 12 mm. Argon gas with a purity of 99.999% with a fixed flow rate of 1.5 standard liters per minute (SLM) was guided over the *n*-hexane to direct *n*-hexane vapors to the plasma gap. The consumption rate of the *n*-hexane precursor was 1 ml per min. In this way, the working gas mixture was achieved. The flow rate of the Ar/C₆H₁₄ gas mixture was monitored by a mass flow controller (Seven stars D07-19B) and a flow readout box (Seven star D08-1F). The frequency of the power supply was 6.5 kHz. Applied voltage and discharge current of the CAP were simultaneously measured by using a high voltage probe (Tektronix P6015A) and a wideband current monitor

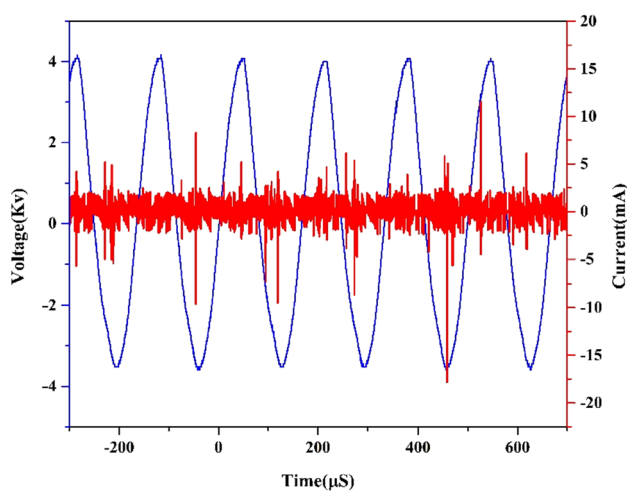


Fig. 2 The voltage and current profiles versus time

(Pearson Electronics, Inc. model 3972), respectively. The voltage and current profiles of the CAP were recorded by using a digital oscilloscope (GW Instek GDS-3354). Optical emission spectroscopy was used to identify the species formed in the CAP system. The optical emission spectra were measured by a compact wide-range (190–1100 nm) spectrometer (Ocean optic, HR2000+CG). For this purpose, the optical fiber was placed at a distance of 1 cm from the copper tube electrode. The silk threads passed through the plasma gap by a take-up roll.

2.2 Sample preparation

Before the deposition, the silk was ultrasonically cleaned in three stages: immersed in ethanol 99%, in acetone 99%, and deionized water, for 10 min. Then the samples were dried at a temperature of 40° for 15 min.

2.3 Surface characterization

The surface morphologies of the untreated and plasma-treated silk were investigated by field emission scanning electron microscope (FESEM) (MIRA3 TESCAN-XMU) at a variety of magnifications. The energy-dispersive spectroscopy (EDS) and X-map analyses were used to investigate the local distribution of the constituent atoms.

Atomic force microscopy (DME Navigator 220) equipped with a DS95 SPM scanner was used to analyze the sample roughness. The image was taken in non-contact mode and different areas of the sample were scanned for each image. The cantilever has an aluminum coating with rectangular geometry. The tip is conical with a height of 15–20 μm, angles less than 20°, and curvature radius less than 10 nm.

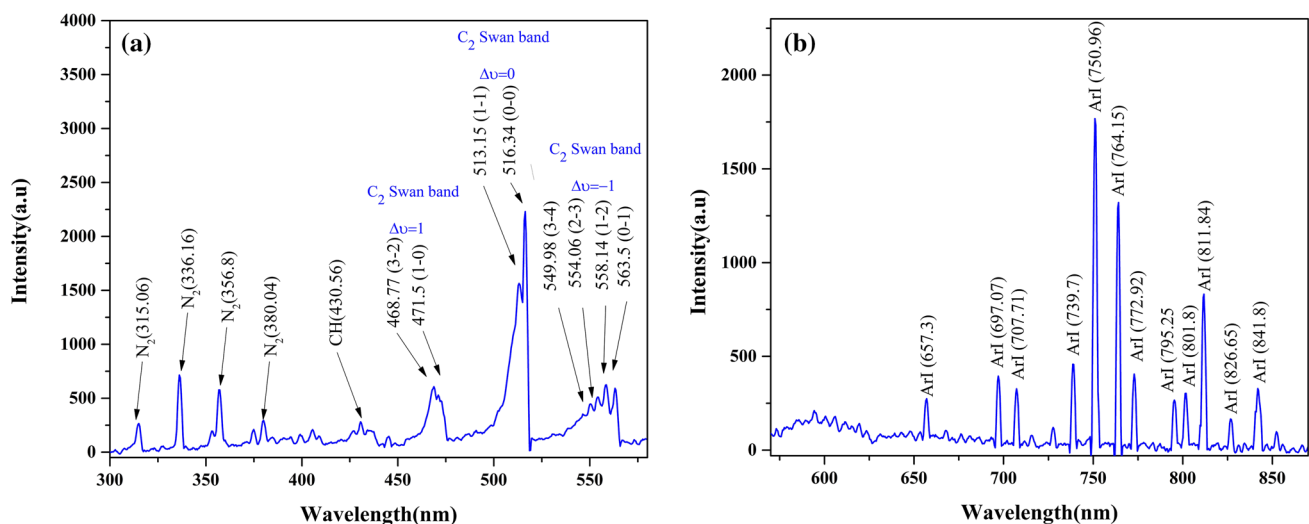
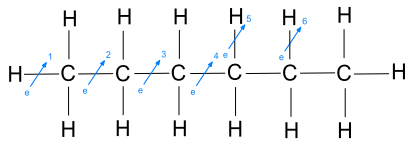
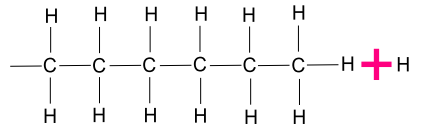
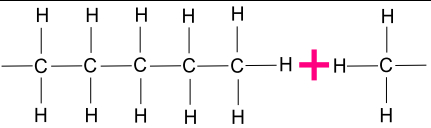
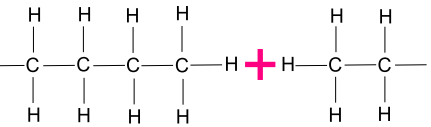
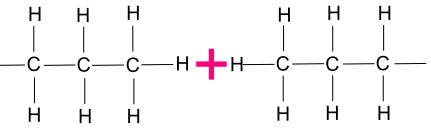
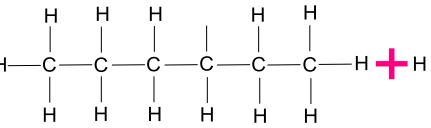
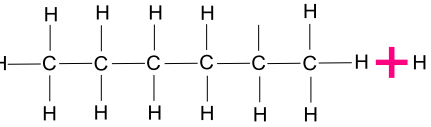


Fig. 3 The optical emission spectrum of atmospheric cold plasma at **a** 300–580 nm, **b** 580–875 nm

Table 1 Initial reactions of *n*-hexane dissociation by electron impacts in the CAP

n-hexane chemical structure (C_6H_{14})		Products	Chemical structures
	1	C_6H_{13}, H	
	2	C_5H_{11}, H_3	
	3	C_4H_9, C_2H_5	
	4	C_3H_7, C_3H_7	
	5	C_6H_{13}, H	
	6	C_6H_{13}, H	

The resonance frequency is 150–190 kHz and the forces are constant, 25–60 N/m.

The chemical bonds of the surface of samples were measured by X-ray photoelectron spectroscopy (X-ray 8025-BesTec XPS system, Germany). The anode material is aluminum and the X-ray source is Al K α X-ray with the energy of 1486.6 eV. The working pressure is 10^{−10} mbar.

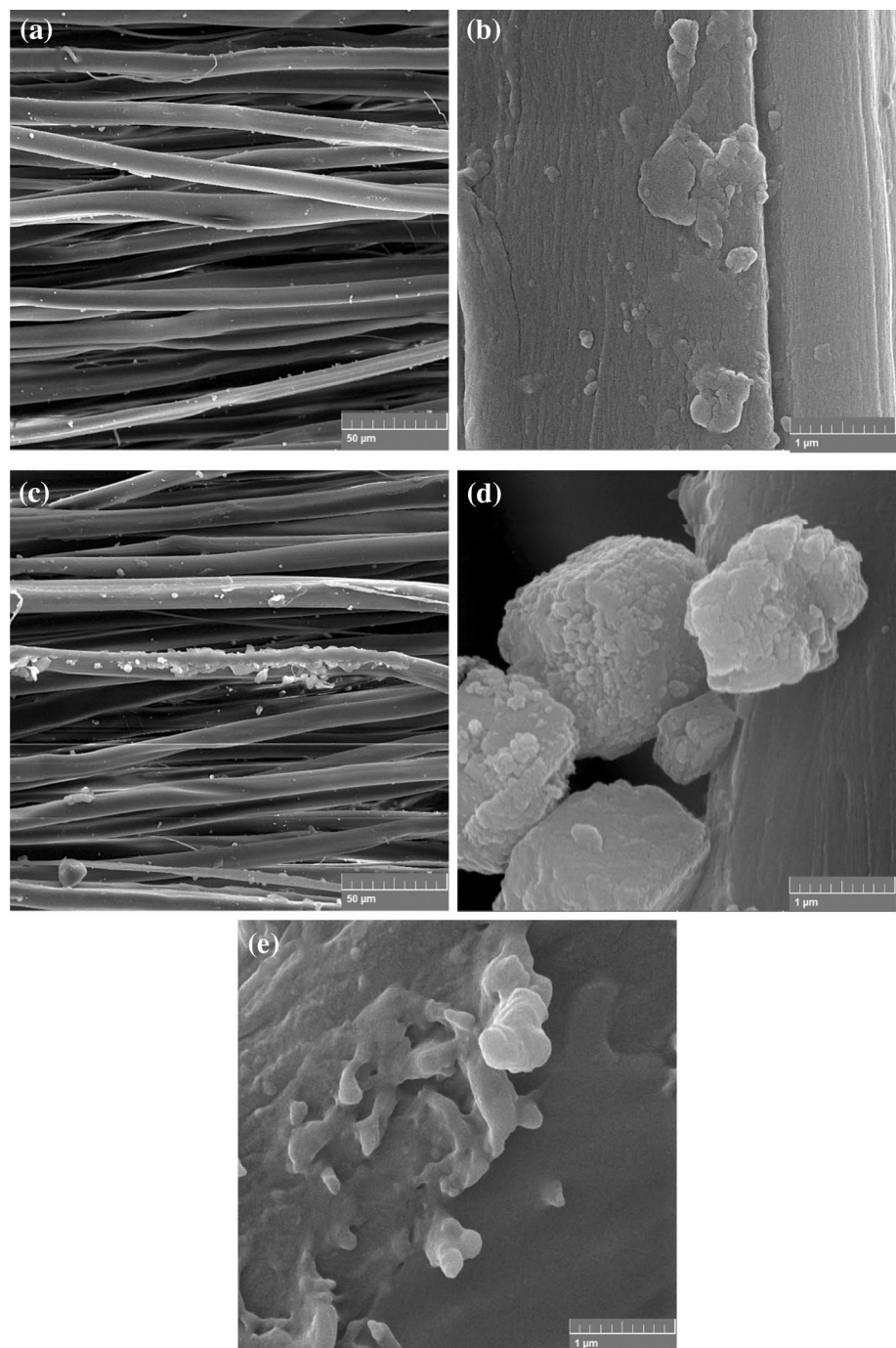
The hydrophobicity of a surface can be interpreted by the contact angle between the droplets of deionized water with the surface itself. The deionized water drops on the hydrophobic surface keep their semi-spherical shape with contact angle more than 90°. If the contact angle is larger than 150°, the surface is called superhydrophobic. On the other hand, the deionized water droplets smeared on the surface of the hydrophilic materials. In this case, the contact angle is less than 90°. The interaction of water droplets with a surface can

be interpreted by surface free energy and surface geometrical structure. A surface with higher energies results in hydrophilicity behavior, while a surface with low energy exhibits hydrophobicity properties.

The roughness (the topographic structure) can affect both the hydrophobicity and hydrophilicity properties. Cassie modeled the roughness effects in terms of air trapping in the hollow area and formation of air–water interfaces, which would enhance hydrophobicity [15].

The static water contact angle measurement was used to determine the hydrophobic property of the deposited silk. For this purpose, we used a 3 μ L droplet of the deionized water at atmospheric pressure and room temperature. The aging effect of hydrophobicity of the treated sample was performed for about 60 days by water contact angle measurements. Wash withstanding durability of the silk fabric was determined in

Fig. 4 FESEM images of the silk fabric: **a, b** pristine samples; **c, d** plasma-treated samples, **e** cotton fabric treated by the dielectric barrier discharge plasma (best sample of reference [14]) scale bar: 50 μm and 1 μm



an aqueous non-ionic detergent solution with a concentration of 1 g per liter in 50 °C temperature for 50 washing cycles. It should be noted that all water contact angle values reported are the average of ten consecutive measurements per sample and we reported the means and standard derivation of the samples.

The color measurement of the samples was performed by using the Dino Capture Lite camera (AM3111-ANMO Electronics Co). The CIELAB color coordinate was employed to analyze any changes in the color of the samples after the plasma processing. The total color difference between the

pristine and the plasma-treated samples was calculated by ΔE^* values. It is a key parameter for calculating the color change of samples. The ΔE^* values are given by the following equations.

$$\Delta E^* = \sqrt{(\Delta L^*)^2 + (\Delta a^*)^2 + (\Delta b^*)^2}$$

$$(\Delta L^*)^2 = L^*_{\text{plasma-treated sample}} - L^*_{\text{untreated sample}}$$

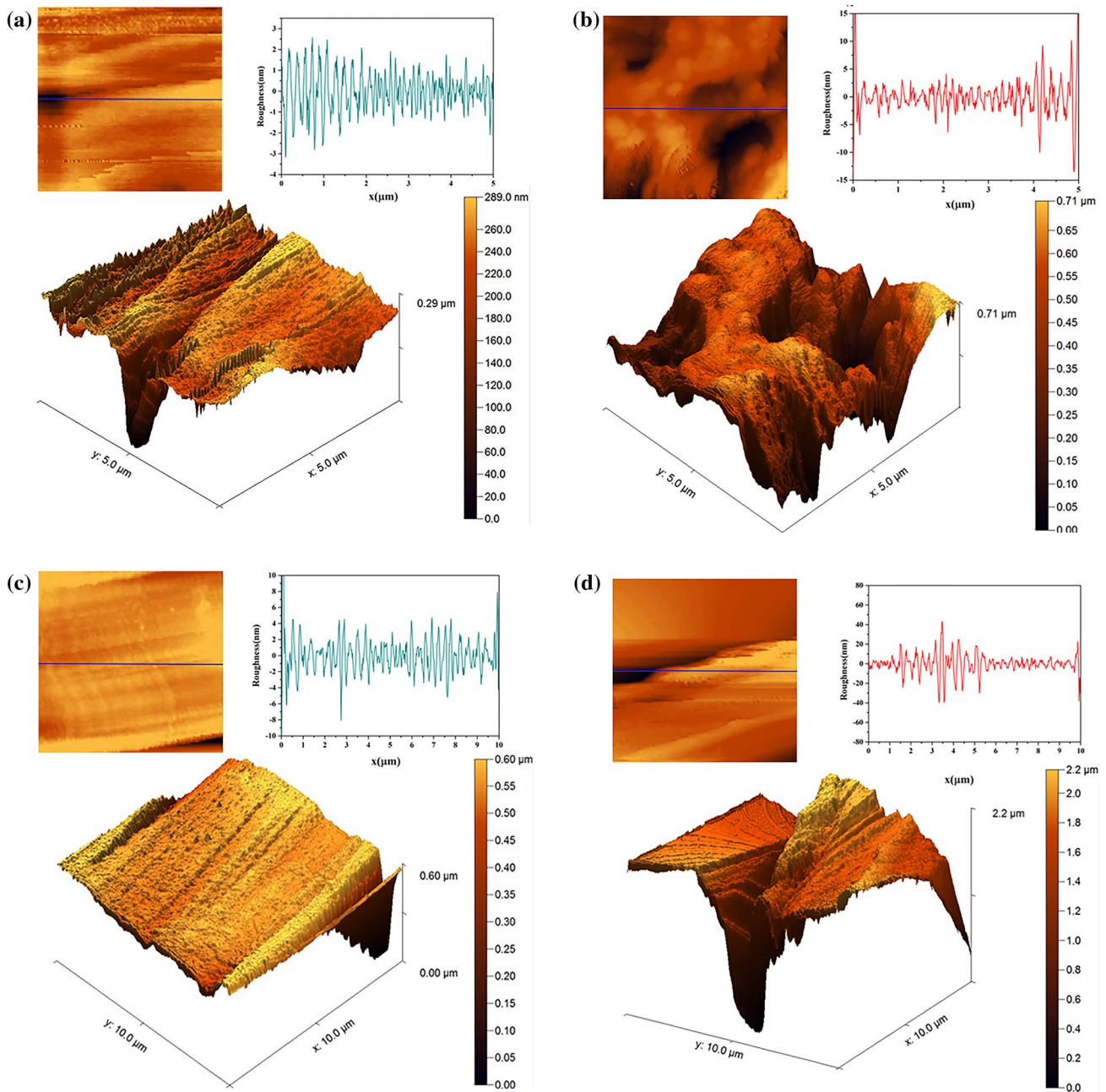


Fig. 5 2D, 3D image and roughness diagram of **a** pristine silk thread at $5\mu\text{m} \times 5\mu\text{m}$, **b** plasma-treated silk thread at $5\mu\text{m} \times 5\mu\text{m}$ scan area, **c** pristine silk thread at $10\mu\text{m} \times 10\mu\text{m}$, **d** plasma-treated silk thread at $10\mu\text{m} \times 10\mu\text{m}$ scan area

$$(\Delta a^*)^2 = a^*_{\text{plasma-treated sample}} - a^*_{\text{untreated sample}}$$

$$(\Delta b^*)^2 = b^*_{\text{plasma-treated sample}} - b^*_{\text{untreated sample}}$$

The whiteness of the samples is calculated by the following equation:

$$\text{Whiteness} = 100 - \sqrt{(100 - L^*)^2 + (a^*)^2 + (b^*)^2}$$

Also, the changes in L^* , a^* and b^* components, and changes in the Whiteness of the samples after the plasma treatment were calculated by statistical analysis T test. The T test is a type of inferential statistical analysis used to determine the significant difference between the means of two groups.

Table 2 Averaged and RMS roughness of the samples at $5\mu\text{m} \times 5\mu\text{m}$ and $10\mu\text{m} \times 10\mu\text{m}$ scanning area

Scale	Sample	RMS roughness (nm)	Averaged roughness (nm)
5 μm	Pristine silk thread	31.8	23.7
	Plasma-treated silk thread	107	87.3
10 μm	Pristine silk thread	52.8	35.6
	Plasma-treated silk thread	298	207
5 μm	Pristine cotton fabric	7.46	9.84
	Plasma-treated cotton fabric	16.4	21.7

Table 3 Relative chemical composition and the atomic ratio of the untreated and plasma-treated silk threads

	Chemical composition			Atomic ratio	
	C1s%	O1s%	N1s%	C/O	C/N
Pristine silk thread	0.41	0.37	0.22	1.108	1.863
Plasma-treated silk thread	0.47	0.34	0.19	1.382	2.473

The mechanical properties of the samples were determined using tensile strength, elongation, and max load (Micro 350 Universal Testing Machine, Shirley). The sensor weight was 250 kg and analysis was performed on ten random points of samples.

3 Results

3.1 Plasma characterization

3.1.1 Electrical characterization

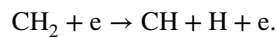
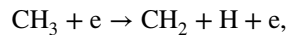
The voltage and current characterizations of the CAP working with Ar/*n*-hexane precursors are shown in Fig. 2. The electric power deposited on the plasma was 1.8 W.

3.1.2 Optical emission spectroscopy

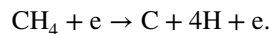
To identify the species formed in the plasma system, we used optical emission spectroscopy as shown in Fig. 3a, b. The spectrum of CAP confirmed the influence of the gas discharge on *n*-hexane decomposition. Figure 3a indicates the spectra lines from 300 to 580 nm in the C₂ and CH band regions. As can be observed in this figure, the C₂ signature exists in the plasma system region. These C₂ lines belong to C₂ swan bands for the transition between $a^3\pi_u$ and $d^3\pi_g$ electronic states of C₂ molecule

with $\Delta v = 1, 0, -1$ [13, 16, 17]. We can also observe the CH radical at 430.56 nm for the transition between $A^2\Delta$ and $X^2\pi$. The initial products of the *n*-hexane decomposition by electron impacts are shown in Table 1. As can be seen from the chemical structure of *n*-hexane, there are six initial reactions for the decomposition of *n*-hexane by electron impacts. The blue arrows show the location of the *n*-hexane dissociation.

In this CAP, the CH radical can be formed through extensive dehydrogenation of methyl radicals via multiple electron impact excitations:



The C and H radicals can be formed through extensive dissociation of the CH₄ molecule [18, 19].



There are also three nitrogen peaks at the plasma region (315.06, 336.16, 356.8, and 380.04 nm) [20]. This N₂ emission line comes from the impurities of the argon/*n*-hexane mixture. In Fig. 3b, argon emission lines can be seen in the range of 570–875 nm.

3.2 Characterizations of the processed samples

3.2.1 Field emission scanning electron microscopy (FESEM)

The surface morphology of the plasma-treated silk thread was probed with field emission scanning electron microscopy (FESEM). Figure 4a, b shows the FESEM image of the pristine silk thread at two different magnifications. As can be seen in this figure, the surface morphology of the untreated samples is quite smooth with neutral microgrooves. Figure 4c, d displays the FESEM image of the silk thread after treatment having some microstructures. This microstructure is due to the deposition of the carbon chemical group on the surface morphology of silk thread with a random distribution.

Also, to compare the results with that of reference [14], we illustrated the FESEM image of the best sample of that reference in Fig. 4e. As can be seen in this figure, the structures deposited on the surface of cotton fabric samples are finer than those of the current work.

3.2.2 Atomic force microscopy (AFM)

To investigate and further ascertain the morphology and changes in the roughness of the plasma-treated silk threads, atomic force microscopy was used. The results are shown in Fig. 5. As can be seen in these images, the surface of

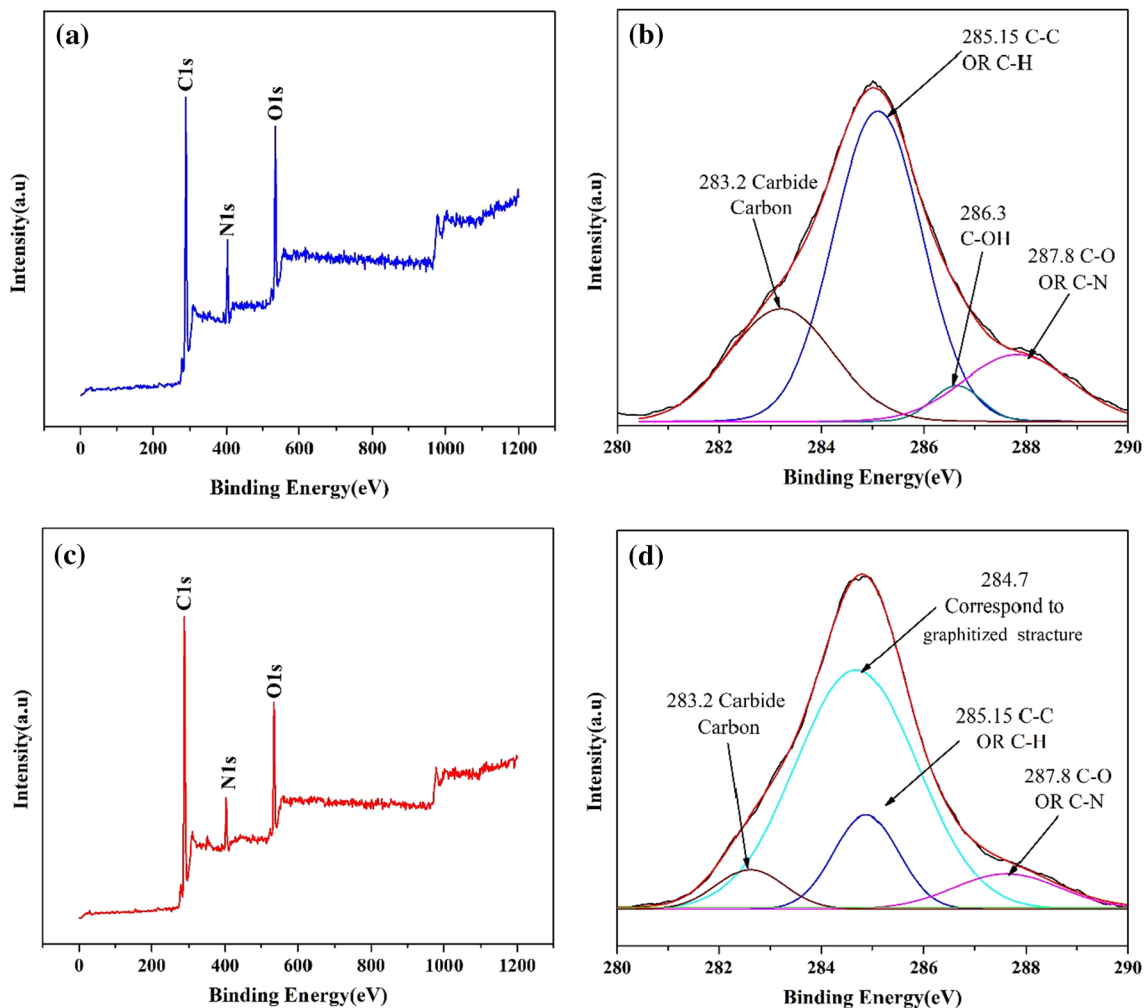


Fig. 6 **a** XPS survey spectra of the pristine silk thread, **b** XPS C1s spectra of the pristine silk, **c** XPS survey spectra of the plasma-treated silk thread, and **d** XPS C1s spectra of the plasma-treated silk thread

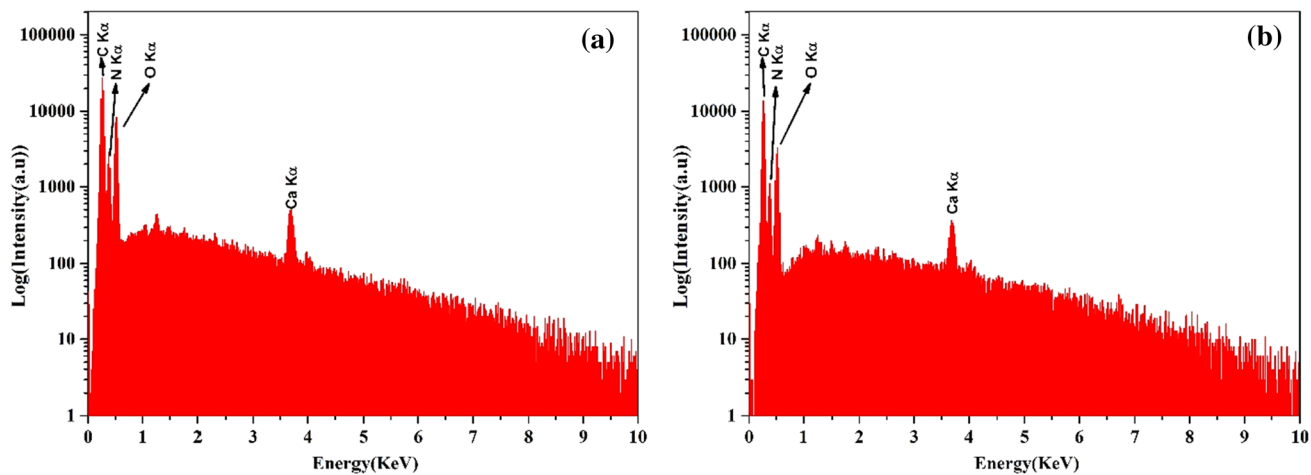


Fig. 7 EDAX analysis of **a** pristine and **b** plasma-treated silk threads

Table 4 The weight and atomic percentage of the carbon, oxygen and nitrogen elements of pristine and plasma-treated silk threads

	Weight percentage%		Atomic percentage%	
	Pristine silk thread	Plasma-treated silk thread	Pristine silk thread	Plasma-treated silk thread
C	39.09	41.88	45.51	48.72
O	17.15	16.00	17.12	15.96
N	42.06	39.33	36.77	34.35

the untreated samples appeared to be flatter compared to plasma-treated samples. The root-mean square (RMS) and the averaged roughness of the samples are detailed in Table 2. It was found that the RMS roughness of the silk threads was increased from 52.8 nm to 298 nm after 60 s of plasma treatments over the $10\mu\text{m} \times 10\mu\text{m}$ scanning area. This increase can be attributed to the formation of fine structures on the surface of the silk as confirmed by the FESEM results.

As can be seen in Table 2, by comparing the roughness of the treated silk with that of cotton over a $5\mu\text{m} \times 5\mu\text{m}$ scanning area, it is revealed that the surface roughness of the silk samples is much more than that of the cotton fabric. The pristine cotton samples were also flattened in the previous work. The increment in the roughness of treated silk thread is due to an increase in the size of the deposited structures on the surface as confirmed by FESEM results.

3.2.3 X-ray photoelectron spectroscopy (XPS)

The chemical composition of the samples was analyzed by X-ray photoelectron spectroscopy (XPS). The results are listed in Table 3. Comparing the two samples shows that there is an obvious increase in the C/O and C/N atomic ratio on the surface of the silk thread after the deposition

[14, 21]. This increase suggests that a new carbon-containing group formed on the surface of the silk thread after the plasma treatments. Also, the results of the best sample in reference [14] showed that plasma deposition led to significant decreases in O1s and increases in C1s spectra after the plasma treatment.

Also, the C1s spectra corresponding to the carbon functionalities group on the surface of the silk thread were investigated to obtain additional insights into the chemical composition of the surface. The results are shown in Fig. 6. Before the performance, the C1s spectra of the samples were deconvoluted and the Shirley backgrounds subtracted. The subtraction is an appropriate approximation for removing the background signals not belonging to the peak. Figure 6b shows the C1s spectrum of the pristine samples. The peak at 285.15 eV corresponds to C–C and C–H, 286.3 eV corresponds to C–OH, and 287.8 eV corresponds to C–O and C–N compounds [13, 14, 22–25]. Figure 6d shows the C1s spectrum of the plasma-treated sample. As can be seen in this image, one peak appeared at 284.7 eV that related to the graphitized structures (the results are the same with previous works) [26].

3.2.4 Energy-dispersive X-ray spectroscopy (EDX)

The composition of the untreated and plasma-treated silk thread was analyzed by an energy-dispersive X-ray spectrometer. The typical spectrum of the samples is shown in Fig. 7. As can be seen in this figure, both samples consisted of carbon, oxygen, and nitrogen. The atomic and weight percentages of carbon, oxygen, and nitrogen atoms on the surface of the samples are given in Tables 4 and 5. According to the results, the plasma-treated samples consisted of a higher percentage of carbon and a lower percentage of oxygen and nitrogen. This suggests that as a result of plasma deposition, a new carbon-containing

Table 5 Aging effect and washing durability of the treated thread

	Aging effect			Washing durability		
	Aging day	Water contact angle	SD	Washing cycles	Water contact angle	SD
1		139.62	5.039	5	133.349	5.704
3		134.559	5.299	10	134.546	4.813
7		136.371	7.40	15	130.565	5.514
10		133.196	5.721	20	132.745	4.679
14		132.423	4.176	25	133.0157	5.138
21		135.372	3.551	30	132.663	5.620
28		133.194	4.514	35	132.861	5.398
35		130.313	5.846	40	132.436	3.373
50		133.400	6.544	45	129.252	5.261
60		134.369	4.559	50	132.666	3.628

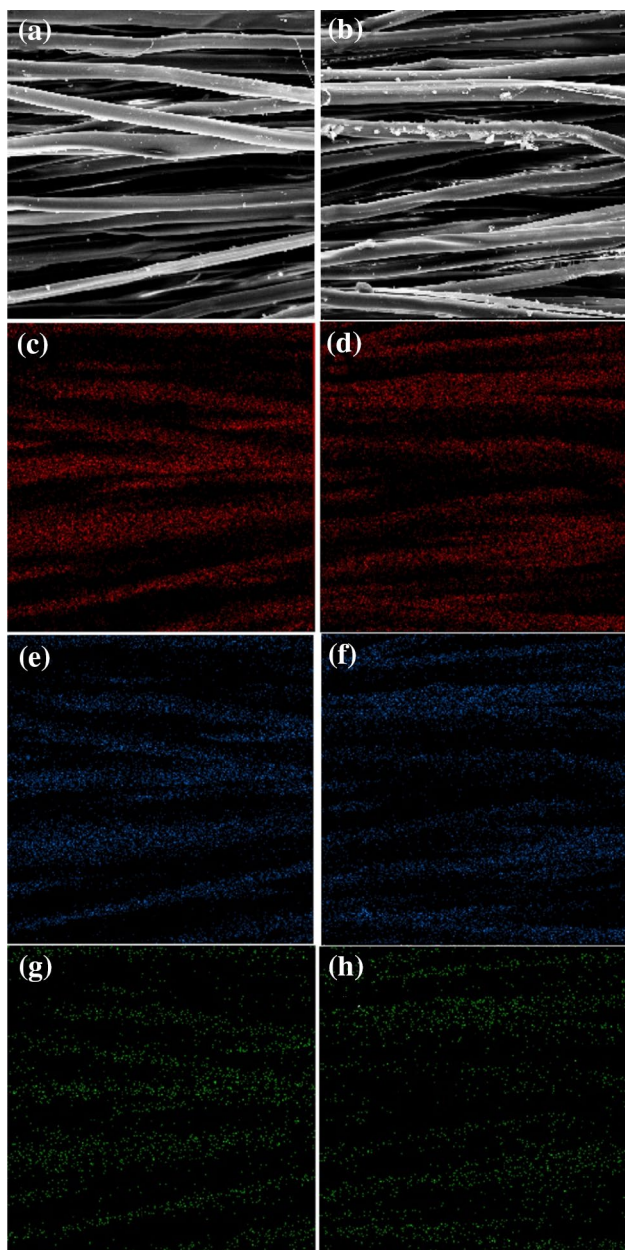


Fig. 8 The carbon (red points), oxygen (blue points) and nitrogen (green points) distribution on the surface of the silk thread for the **a, c, e, g** pristine and **b, d, f, h** plasma-treated samples

group formed on the surface of the silk thread that completely confirmed the XPS result.

3.2.5 Elemental map analysis

To study the local distribution of the carbon, oxygen, and nitrogen atoms on the silk surface, the elemental map analysis was performed. Figure 8 displays the carbon, oxygen, and nitrogen atom distributions on the silk surface. The results showed that plasma processing led to a slight change in the

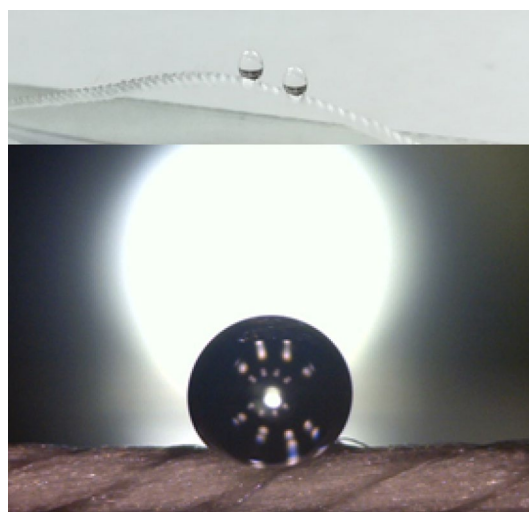


Fig. 9 Water contact angles of plasma-treated silk thread

distribution of carbon, oxygen, and nitrogen content on the surface of the silk thread. The results were supported by EDAX and XPS analysis.

3.2.6 Water contact angles

To investigate the hydrophobicity properties of the samples, the static water contact angle measurement was performed. Generally, if the water contact angle of samples is smaller than 90° , the surface of the samples is considered as hydrophilic, and if it is larger than 90° , the surface is hydrophobic. Furthermore, the samples with water contact angles above 150° are considered as a superhydrophobic sample. Before plasma deposition, the static water contact angles appeared to be about zero degrees. Figure 9 shows the image of the deionized water droplets on the surface of the plasma-treated silk thread. The result showed that the water contact angle reached 139.62° after 60 s of treatment by the CAP. Based on the principles of the wettability theory of Wenzel and Cassie Baxter, increasing surface roughness of solid surface results in an increase in hydrophobicity [26, 27]. Growth in the roughness of the surface in our sample was verified by AFM analysis, so it can be said that the increase in water contact angles of the samples could be due to an increase in surface roughness. Also, the effect of the surface chemistry on wettability cannot be neglected. Based on the results of XPS and EDAX analysis, plasma treatment led to an increase in carbon content and a decrease in oxygen and nitrogen of the surface. Consequently, a decrease in oxygen as a hydrophilic group and an increase in carbon as a hydrophobic group on the surface led to the improvement in hydrophobicity properties of the treated silk threads (which was confirmed by XPS C1s spectrum results). The water contact angle of the best sample in this work and that of

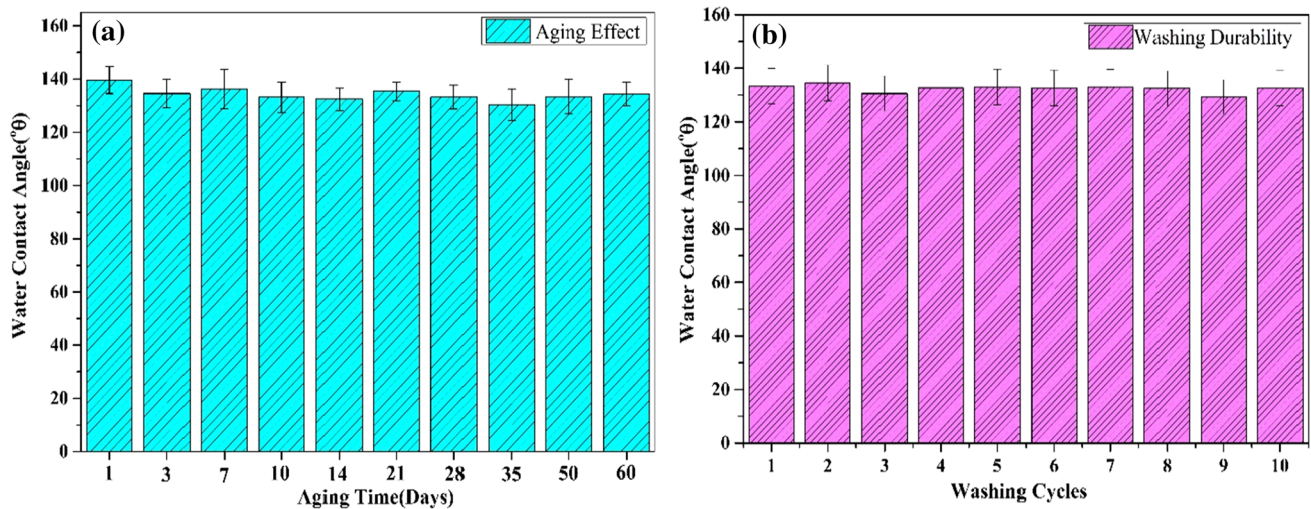


Fig. 10 Aging effect and washing durability of the treated thread

Table 6 Indications for the color changes of the silk threads

	Number of tests	mean	SD	Sig
L^* component of pristine silk thread	20	49.83	6.01	0.247
L^* component of plasma-treated silk thread	20	49.14	8.88	
a^* component of plasma pristine silk thread	20	-0.13	2.10	0.143
a^* component of plasma-treated silk thread	20	0.43	1.49	
b^* component of plasma pristine silk thread	20	-1.28	3.02	0.690
b^* component of plasma-treated silk thread	20	-1.94	3.28	

reference [14] were 139.62 and 159.59°, respectively. The greater value is due to a significant decrease in O1s peak

(hydrophilic group on the surface of the samples confirmed by XPS analysis).

3.2.7 Aging effect and washing durability of the samples

To investigate withstanding of the hydrophobic properties of the plasma-treated samples versus time, water contact angle measurements were performed up to 60 days. It was revealed that the static water contact angle of the treated samples reduced by about 5-degrees for two months after treatment by CAP. Besides, washing durability of the plasma-treated samples was investigated by measuring the water contact angles. According to the results, the static water contact angles of the treated samples show a 7° reduction after 50 cycles of washing (Fig. 10).

3.2.8 Color test

CIELAB color space $L^*a^*b^*$ was used to calculate color changes of the treated silk threads. The details of the color

Fig. 11 The image of a pristine and b plasma-treated silk threads

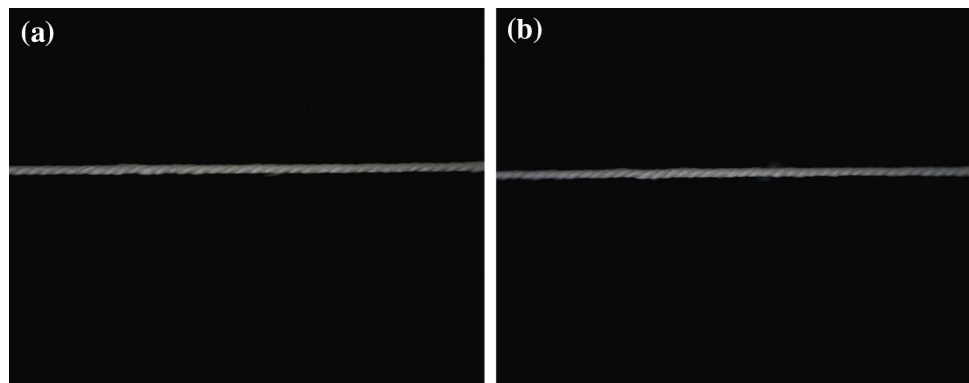


Table 7 Whiteness changes of silk threads

	Number of tests	Mean	SD	Sig
Pristine silk thread	20	49.68	5.94	0.289
Plasma-treated silk thread	20	48.99	8.94	

examinations were presented in our previous work [14]. To evaluate color changes of the silk thread, 20 random measurements were made for each sample and color change calculated with the *T* test. The results are shown in Table 6.

According to the results, there was no significant change in L^* , a^* , and b^* values after a 60 s processing of the silk thread. The total color difference between the pristine and the plasma-treated samples can be calculated from the ΔE^* values [14]. The calculated ΔE^* of samples is 1.01. The calculated ΔE^* of the best samples in previous work is 6.137. This shows that the CAP tool did not change the color of the silk thread and had better results compared to the previous works. Figure 11 displays the color of the untreated and the plasma-treated silk thread. Both samples' whiteness are shown in Table 7. The results showed that there was not a significant change in the whiteness of the treated sample.

3.2.9 Mechanical properties

In this study, the breaking strength, elongation, and extension properties of plasma-treated silk threads were investigated in comparison to pristine silk. For each sample, ten random measurements were performed and the mean and standard deviation of measurements was reported. The results are shown in Table 8. As can be seen from Table 8, there was a slight increase in breaking strength, elongation, and extension after the plasma processing. This increase could be attributed to an increase in the surface roughness of the processed samples [3, 28–30].

Table 8 Tensile strength of untreated and plasma-treated silk threads

		Number of tests	Mean	SD
Breaking strength (cN)	Pristine silk thread	10	538.28	40.17
	Plasma-treated silk thread	10	565.40	37.18
Elongation (mm)	Pristine silk thread	10	8.05	0.706
	Plasma-treated silk thread	10	8.66	1.024
Extension (%)	Pristine silk thread	10	16.11	1.414
	Plasma-treated silk thread	10	17.317	2.051

4 Conclusions

In conclusion, we introduced a low-cost and environmentally friendly approach for modifying silk thread with ordinary hydrophilic property to a hydrophobic thread without any change in the bulk. In this work, we used a new geometry of electrodes in a cold atmospheric pressure plasma to deposit a hydrophobic coating on silk thread with Ar/C₆H₁₄ mixture. The new apparatus is more efficient and has many advantages compared to the previous ones [14]. The process of silk thread treatment is faster than that of reference [14], single-step, roll to roll, and it could be used in the textile industry to produce functional silk fabrics. The device is compact and could be installed before or after dyeing the fibers in the factory for the functionalization of different types of fibers, too. The color changes of the samples processed by the newly developed device were lower than those of cotton fabric which was processed by a DBD device. Furthermore, the breaking strength, elongation, and extension of the silk threads increased after the plasma processing.

The FESEM probe showed that our processing deposited nanometer to micrometer structures on the surface of the samples. AFM analysis proved that the roughness of the treated silk samples was increased, noticeably, which in turn made the samples to be a hydrophobic material.

The results of the XPS analysis proved that new carbon bonds have been formed on the surface of the samples. It was revealed that there is a 24.7% increase in the C/O and a 32.7% increase in the C/N content ratio on the silk surface after the plasma processing. This increase in C/O and C/N content ratio suggests that a new carbon-containing group formed on the surface of silk thread after the plasma treatments. A comparison between the C/O percentage in the treated silk and cotton fabric indicates that the treated silk threads possess a much lower C/O ratio.

EDAX analysis showed an increase in carbon and a decrease in nitrogen and oxygen contents of the surface that completely confirmed the results of XPS. The hydrophobicity of the silk thread was shown by SWCA to be 139.62°. This value is lower than that of cotton fabric due to the lower C/O ratio on the surfaces. The durability of

the hydrophobicity property of the processed silk was almost the same versus time and 50 washing cycles. The color of the treated silk did not significantly change after the plasma deposition. Finally, the mechanical properties such as breaking, strength, elongation, and extension were found to be increased after plasma processing. The results of this work could lead to the production of self-cleaning and water-repellent silk fabrics, including carpets, blankets, and dresses with a low-cost treatment stage.

References

- X.S. Liu, T.L. Xing, D.M. Xu, G.Q. Chen, *Chin. Chem. Lett.* **23**, 665 (2012)
- M.D. Teli, K.K. Samanta, P. Pandit, S. Basak, T.N. Gayatri, *Int. J. Bio-resour. Sci.* **2**, 15 (2015)
- S. Li, D. Jinjin, *Appl. Surf. Sci.* **253**, 5051 (2007)
- S.K. Hodak, T. Supasai, B. Paosawatyanong, K. Kamlangkla, V. Pavarajarn, *Appl. Surf. Sci.* **254**, 4744 (2008)
- J. Ryu, K. Kim, J. Park, B.G. Hwang, Y. Ko, H. Kim, J. Han, E. Seo, Y. Park, S.J. Lee, *Sci. Rep.* **7**, 1981 (2017)
- J. Zimmermann, F.A. Reifler, G. Fortunato, L.C. Gerhardt, S. Seeger, *Adv. Funct. Mater.* **18**, 3662 (2008)
- C. Zhang, F. Guo, H. Li, Y. Wang, Z. Zhang, *Appl. Surf. Sci.* **490**, 197 (2019)
- K.V. Rani, N. Chandwani, P. Kikani, S.K. Nema, A.K. Sarma, B. Sarma, *Surf. Rev. Lett.* **25**, 1850060 (2018)
- J. Zhang, P. France, A. Radomyselskiy, S. Datta, J. Zhao, W. Van Ooij, *J. Appl. Polymer. Sci.* **88**, 1473 (2003)
- F. Hochart, R. De Jaeger, J.L. Grützmacher, *Surf. Coat. Technol.* **165**, 201 (2003)
- M. Lee, Y.G. Ko, J.B. Lee, W.H. Park, D. Cho, O.H. Kwon, *Macromol. Res.* **22**, 746 (2014)
- Y.G. Ko, M. Lee, W.H. Park, D. Cho, O.K. Kwon, O.H. Kwon, *Macromol. Res.* **24**, 824 (2016)
- F. Sohbatzadeh, E. Shakerinasab, M. Eshghabadi, M. Ghasemi, *Diam. Relat. Mater.* **91**, 34 (2019)
- F. Sohbatzadeh, M. Farhadi, E. Shakerinasab, *Surf. Coat. Technol.* **374**, 944 (2019)
- A.B.D. Cassie, S. Baxter, *Trans. Faraday Soc.* **40**, 546561 (1944)
- S.S. Harilal, R.C. Issac, C.V. Bindhu, V.P.N. Nampoory, C.P.G. Vallabhan, *J. Phys. D Appl. Phys.* **30**, 1703 (1997)
- K.F. Al Shboul, S.S. Harilal, A. Hassanein, *J. Appl. Phys.* **113**, 163305 (2013)
- J.H. Yan, Z. Bo, X.D. Li, C.M. Du, K.F. Cen, B.G. Cheron, *Plasma. Chem. Plasma. Process.* **27**, 115 (2007)
- C. Boyadjian, A. Ağiral, J.G. Gardeniers, L. Lefferts, K. Seshan, *Plasma. Chem. Plasma. Process.* **31**, 291 (2011)
- M.K. Boudam, B. Saoudi, M. Moisan, A. Ricard, *J. Phys. D Appl. Phys.* **40**, 1694 (2007)
- V.N. Vasilets, A. Hirose, Q. Yang, A. Singh, R. Sammynaiken, M. Foursa, Y.M. Shulga, *Appl. Phys. A* **79**, 2079 (2004)
- T. Topalovic, V.A. Nierstrasz, L. Bautista, D. Jovic, A. Navarro, M.M. Warmoeskerken, *Coll. Surf. A Phys. Eng. Aspe.* **296**, 76 (2007)
- P. Fardim, A.H. Hulten, J.P. Boisvert, L.S. Johansson, M. Ernsts-son, J.M. Campbell, A. Lejeune, B. Holmbom, J. Laine, D. Gray, *Holzforchung* **60**, 149 (2006)
- J. Profili, O. Levasseur, N. Naudé, C. Chaneac, L. Stafford, N. Gherardi, *J. Appl. Phys.* **120**, 053302 (2016)
- F. Sohbatzadeh, M. Eshghabadi, T. Mohsenpour, *Nanotechnology* **29**, 265603 (2018)
- V. Datsyuk, M. Kalyva, K. Papagelis, J. Parthenios, D. Tasis, A. Siokou, I. Kallitsis, C. Galiotis, *Carbon* **46**, 833 (2008)
- R.N. Wenzel, *Ind. Eng. Chem.* **28**, 988994 (1936)
- Y. Yao, S. Chen, *J. Compos. Mater.* **47**, 2909 (2013)
- C.H. Suh, Y.C. Jung, Y.S. Kim, *J. Mech. Sci. Technol.* **24**, 2091 (2010)
- W. Kowbel, C.H. Shan, *Carbon* **28**, 287 (1990)

Publisher's Note Springer Nature remains neutral with regard to jurisdictional claims in published maps and institutional affiliations.